CrossMark

Photocatalytic degradation of methylene blue on TiO$_2$@SiO$_2$ core/shell nanoparticles: synthesis and characterization

Tahereh Gholami[1] · Mehdi Bazarganipour[2] · Masoud Salavati-Niasari[1] · Samira Bagheri[3]

Abstract TiO$_2$@SiO$_2$ core/shell nanoparticles have been synthesized by sol–gel method from tetraethylorthotitanate and tetraethylorthosilicate. The synthesized products were characterized by X-ray diffraction, scanning electron microscopy, Fourier transform infrared spectrum, electron dispersive X-ray spectroscopy and ultraviolet–visible. The results revealed that compared to SiO$_2$ and TiO$_2$, TiO$_2$@-SiO$_2$ core/shell nanoparticles display smaller crystal size and greater band gap energy. The photocatalytic activity of the synthesized products has been compared in the photodegradation activity of methylene blue.

1 Introduction

Dye is a vital chemical used in several industries such as those involved in producing fabric, food, furniture and paint, representing a major threat to the environment due to its toxicity and potentially carcinogenic nature [1, 2].

✉ Mehdi Bazarganipour
  bazarganipour@cc.iut.ac.ir

✉ Masoud Salavati-Niasari
  salavati@kashanu.ac.ir

1   Institute of Nano Science and Nano Technology, University of Kashan, P. O. Box 87317-51167, Kashan, Islamic Republic of Iran

2   Nanotechnology and Advanced Materials Institute, Isfahan University of Technology, 84156-83111 Isfahan, Islamic Republic of Iran

3   Centre for Research in Nanotechnology and Catalysis (NANOCAT), 3rd Floor, Block A, Institute of Postgraduate Studies (IPS), University of Malaya, 50603 Kuala Lumpur, Malaysia

Water purification is one of the most important issues in environmental science [3–9] and synthetic dyes are the main pollutant groups of wastewater [10–13]. Even in low quantities, presence of dyes can cause serious environmental problems, for instance, growth of aquatic bacteria can be inhibited by interference of penetration of sunlight into water by organic dye molecules [10–13]. Therefore, much effort has been made to reduce the concentration of organic dyes in the wastewater [10–17]. Use of photocatalysts has been considered as one of the most promising ways of removing organic compounds from water [8, 12–16].

Among different existing photocatalysts, titanium dioxide has been intensively investigated for their promising mechanical, chemical, electrical, and optical properties. In particular, great attention has been devoted to the study of the photocatalytic properties of TiO$_2$ powders and thin films useful for the purification of air and water and the provision of self cleaning surfaces [18–21]. This activity can be obtained due to its ability to mineralize a wide range of organic contaminants, such as aromatics, alkanes, alcohols, haloalkanes, dyes, insecticides, and surfactants, and to the photo induced super hydrophilic effect.

However, application of TiO$_2$ as a photocatalyst for purification of wastewater can be limited by several factors. First, photocatalytic activity of TiO$_2$ is easily deactivated by deposition of surface-bound carbonate compounds as intermediate products of oxidative decomposition of organic molecules [22–24]. Second, TiO$_2$ can only adsorb UV light due to its wide band gap, and therefore, its photocatalytic efficiency in sunlight is low [25, 26].

Recently, a TiO$_2$@SiO$_2$ mixed oxide was reported to be more active as a photocatalyst than pure titania [27, 28]. The addition of SiO$_2$ to TiO$_2$ enhances the thermal stability of the anatase phase [29] and increases the surface area [30]. Cheng et al. [31] have reported that silica-doped TiO$_2$

has high photocatalytic activity due to the suppression of the anatase to rutile phase transition and the formation of oxygen vacancies.

The procedures utilized for the synthesis $TiO_2@SiO_2$ core/shell nanoparticles include hydrothermal, co-precipitation and sol–gel procedures [32–34]. Among these procedures, the sol–gel procedure is the most method for controlling textural and surface characteristic of nanoparticles [35, 36].

Methyl blue (MB) is a water-soluble dye, which is widely used in the textile, printing, paper manufacturing, pharmaceutical, food industries and also in research laboratories. The safe removal of this kind of dye is the first aim of our present research. In the present paper, MB was chosen as the model dye.

2 Experimental

2.1 Materials and characterization

Tetraethyl orthotitanate (TEOT), tetraethyl orthosilicate (TEOS) and triethanolamine (TEOA) used in our experiments were purchased from Merck. For characterization of the products X-ray diffraction (XRD) patterns were recorded by a Rigaku D-max C III, X-ray diffractometer using Ni-filtered Cu Kα radiation. Scanning electron microscopy (SEM) images were obtained on Philips XL-30ESEM. Fourier transform infrared (FT-IR) spectra were recorded on Shimadzu Varian 4300 spectrophotometer in KBr pellets. Optical analyses were performed using a V-670 UV–Vis–NIR Spectrophotometer (Jasco).

2.2 Preparation of titana nanoparticles

The standard procedure for the preparation of TiO_2 nanoparticles was conducted according to the literature [37, 38]. The solution of Ti^{4+}(0.5 M) which is stable against hydrolysis at room temperature, was prepared by mixing tetraethyl orthotitanate (TEOT) and TEOA with a molar ratio of TEOT:TEOA = 1:2, followed by the addition of distilled water (50 mL). The final pH of solutions was 9.6 and was fixed at this pH by mixing with $HClO_4$ or NaOH solution. The solution was placed in a Teflon-lined autoclave and aged at 100 °C for 24 h for gelation; then, drying was carried out using a conventional oven at 100 °C for 24 h under vacuum for overnight. The samples were calcinated at 600 °C for 2 h.

2.3 Preparation of silica nanoparticles

Silica nanoparticles were synthesized by using modified Stöber process [39–48]. The solution of TEOS (0.5 M) which is stable against hydrolysis at room temperature, was prepared by mixing TEOS and TEOA with a molar ratio of TEOS:TEOA = 1:2, followed by the addition of distilled water (50 mL). The final pH of solutions was 9.6 and was fixed at this pH by mixing with $HClO_4$ or NaOH solution. The solution was placed in a teflon-lined autoclave and aged at 100 °C for 24 h for gelation; then, drying was carried out using a conventional oven at 100 °C for 24 h under vacuum for overnight. The samples were calcinated at 600 °C for 2 h.

2.4 Preparation of $TiO_2@SiO_2$ core/shell nanoparticles (photocatalyst preparation)

The solution prepared by mixing TEOT and TEOA with a molar ratio of TEOT:TEOA = 1:2, followed by the addition of 50 mL distilled water. In continues, TEOS was added to the solution with a molar ratio of TEOT:TEOS = 1:1. The solution was placed in a Teflon-lined autoclave and aged at 100 °C for 24 h for gelation; then, drying was carried out using a conventional oven at 100 °C for 24 h under vacuum for overnight. The samples were calcinated at 600 °C for 2 h.

2.5 Photocatalytic experiment

The photocatalytic activities of the samples were determined by the degradation of aqueous methylene blue (MB) under UV light. About 10 mg of the sample was first inserted to a reactor that included 2×10^{-6} M of aqueous MB. The suspension was transferred into a self-designed glass reactor, and stirred in darkness to attain the adsorption equilibrium. In the research of photodegradation by UV light, a 125 W high-pressure mercury lamp with a water cooling cylindrical jacket was utilized. The concentration of MB was checked on the basis of its UV–visible absorption peak at 664 nm.

3 Results and discussion

3.1 FT-IR spectroscopy

Investigating the surface chemistry of nanoparticles would help to have a better view of their properties (Fig. 1). FT-IR spectrum of TiO_2 samples have been shown in Fig. 1a. The absorption around 3429 and 1630 cm^{-1} are due to the stretching and bending vibration of water molecules, respectively. As shown in Fig. 1a, the broad band in 460 cm^{-1} in the FT-IR spectra of the TiO_2 sample belongs to the characteristic vibrations of the inorganic Ti–O–Ti network [49]. FT-IR spectra of SiO_2 nanoparticles have been shown in Fig. 1b. The spectra show that the peaks
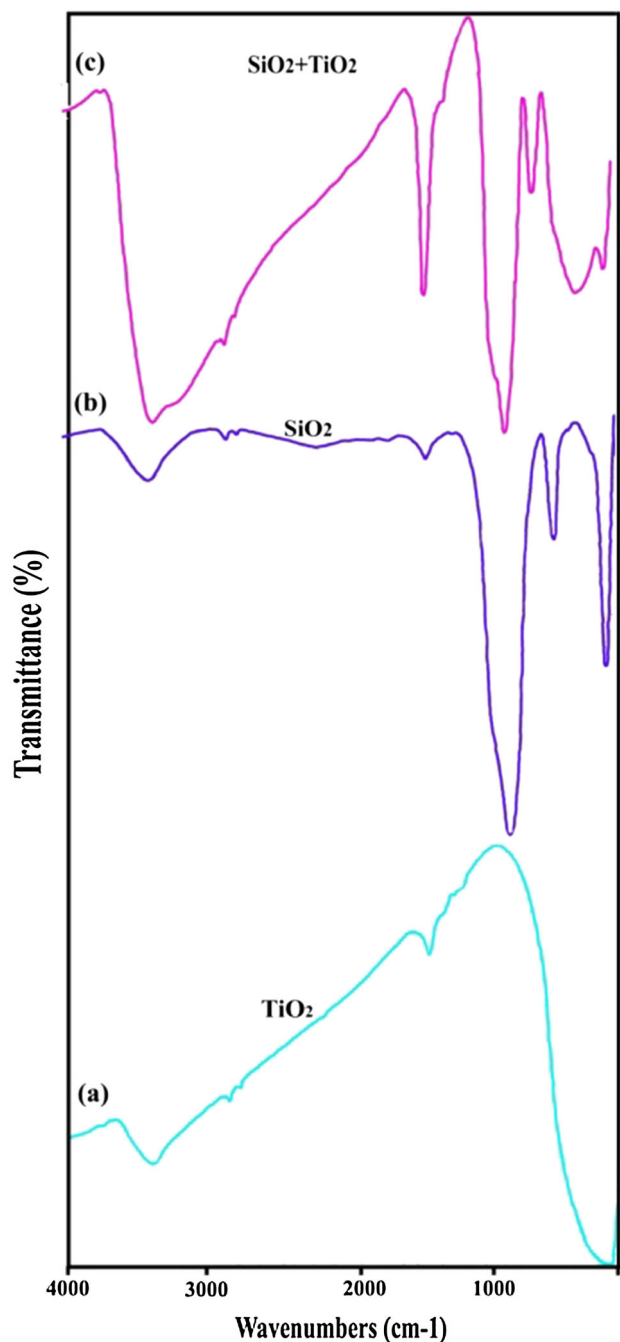
Fig. 1 FT-IR spectra of prepared *a* SiO$_2$, *b* TiO$_2$ and *c* TiO$_2$@SiO$_2$

corresponding to stretching and bending vibration of OH by adsorbed water molecules are 3432 and 1630 cm^{-1}, respectively. Three bands at 472, 807, and 1105 cm^{-1} dominate the spectra for silica sample which are attributed to stretching and bending vibration of silicon and oxygen. The peak at 1105 cm^{-1} corresponds to asymmetric vibrations of O–Si–O, 807 cm^{-1} is ascribed to symmetric stretching vibrations of O–Si–O and the peak at 472 cm^{-1} corresponds to bending vibrations of silica [50]. Figure 1c shows the FT-IR spectra of prepared TiO$_2$@SiO$_2$ core/shell

nanoparticles. The band around 468 cm^{-1} is attributed to the Ti–O–Ti stretching vibration of crystalline TiO$_2$ phase. The band near 1101 cm^{-1} corresponds to the asymmetric stretching vibration of Si–O–Si bond. The bands at around 3390 and 1628 cm^{-1} are attributed to the bending vibration of hydroxyl groups by adsorbed water molecule. Besides, another band around 940 cm^{-1} is commonly accepted as the characteristic stretching vibration of Ti–O–Si bonds, which implies the substitution of Si for Ti occurred to form Si–O–Ti bonds in TiO$_2$@SiO$_2$ core/shell nanoparticles.

3.2 X-ray diffraction patterns

The X-ray diffraction patterns of as-prepared product have been shown in Fig. 2. Figure 2a shows the XRD pattern of SiO$_2$ nanoparticles synthesized by modified Stöber process. This pattern shows the amorphous nature of the prepared sample. The intense peak at $2\theta = 22$ indicates that the SiO$_2$ peak has amorphous nature. No other impurity peaks were present in the SiO$_2$ nanoparticles. As shown in Fig. 2b, all diffraction peaks can be well indexed to pure anatase structural titanium oxide. No peaks of the rutile or
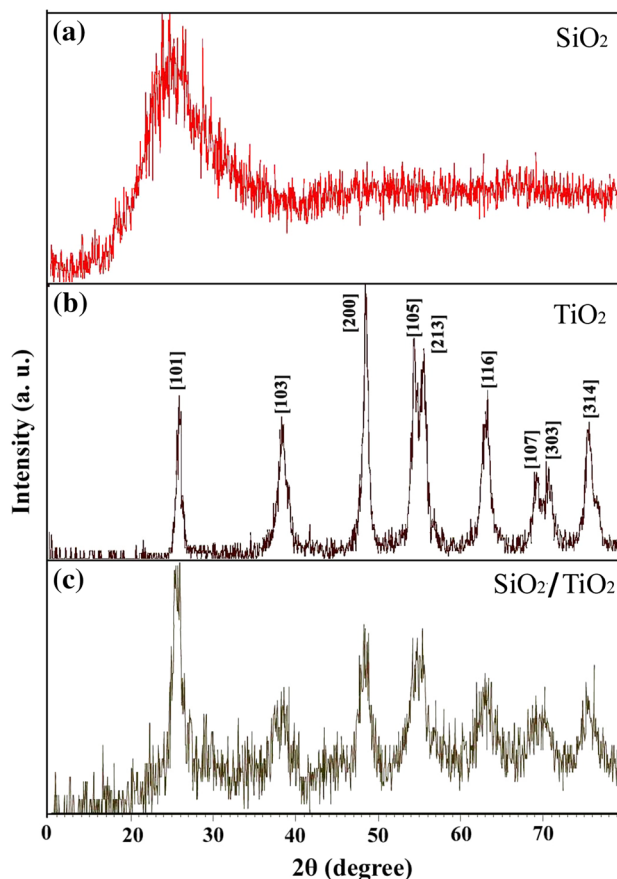

Fig. 2 XRD patterns of prepared **a** SiO$_2$, **b** TiO$_2$ and **c** SiO$_2$@TiO$_2$

brookite phase were detected, indicating satisfactory purity of these products. All the peaks were labeled and can be indexed to JCPDS Card No. 04-0477. Figure 2c shows the XRD pattern of $TiO_2@SiO_2$ core/shell nanoparticles. As shown in Fig. 2c, the profiles show the presence of anatase TiO_2. No other peaks can be observed, which could be attributed to amorphous phase of SiO_2, or Si as an interstitial atom is well-inserted into the crystal lattice of TiO_2.

3.3 SEM images

Figure 3 shows the surface morphology of the synthesized nanoparticles evaluated by scanning electron microscopy. The three different catalysts, SiO_2, TiO_2 and $TiO_2@SiO_2$ core/shell were imaged by SEM (Fig. 3). The SiO_2 nanoparticles is consisted of irregularly shaped particles with a wide size range (25–80 nm), as shown in Fig. 3a. The TiO_2 nanoparticles have non-uniform particles (Fig. 3b) in large clumps (50–250 nm), which was probably due to growth and densification. The TiO_2/SiO_2 core/shell formed relatively uniform particles (20–50 nm) with some nanoagglomerates, as shown in Fig. 3c.

3.4 Optical properties

To investigate the optical absorption properties of prepared samples, the UV–Vis study was carried out (Fig. 4). It is known that the absorption of light affects the photocatalytic activity considerably. The UV–Vis spectrum of the as-prepared SiO_2 nanoparticles has been shown in Fig. 4 (red line). There is a strong absorption peak located at 280 nm, compared with the absorption peak of bulk SiO_2 materials ($E_g \sim 11$ eV) [51]. Figure 4 (blue line) shows UV–Vis spectrum of the as-prepared TiO_2 nanoparticles. This spectrum exhibits the absorption peak located at 314 nm. In addition, it is denoted that the absorption peak (280 nm) in UV–Vis spectrum decreased for $TiO_2@SiO_2$ core/shell compared with SiO_2 and TiO_2 nanoparticles [Fig. 4 (green line)]. This is probably due to the coverage of SiO_2 on TiO_2 surface which restrained the absorption of UV–Vis light. This phenomenon can be explained in terms of the change in band gap energy of TiO_2 due to SiO_2. Many reports concluded that SiO_2 causes the blue shift of TiO_2 by two mechanism; (1) reducing the particle size of TiO_2 due to siliceous framework (quantum size effect) and (2) forming Ti–O–Si bonds leading to the modification of the electronic structure [52–55] (Scheme 1).

The fundamental absorption edge in most semiconductors follows the exponential law. Using the absorption data, the band gap was estimated by Tauc's relationship:
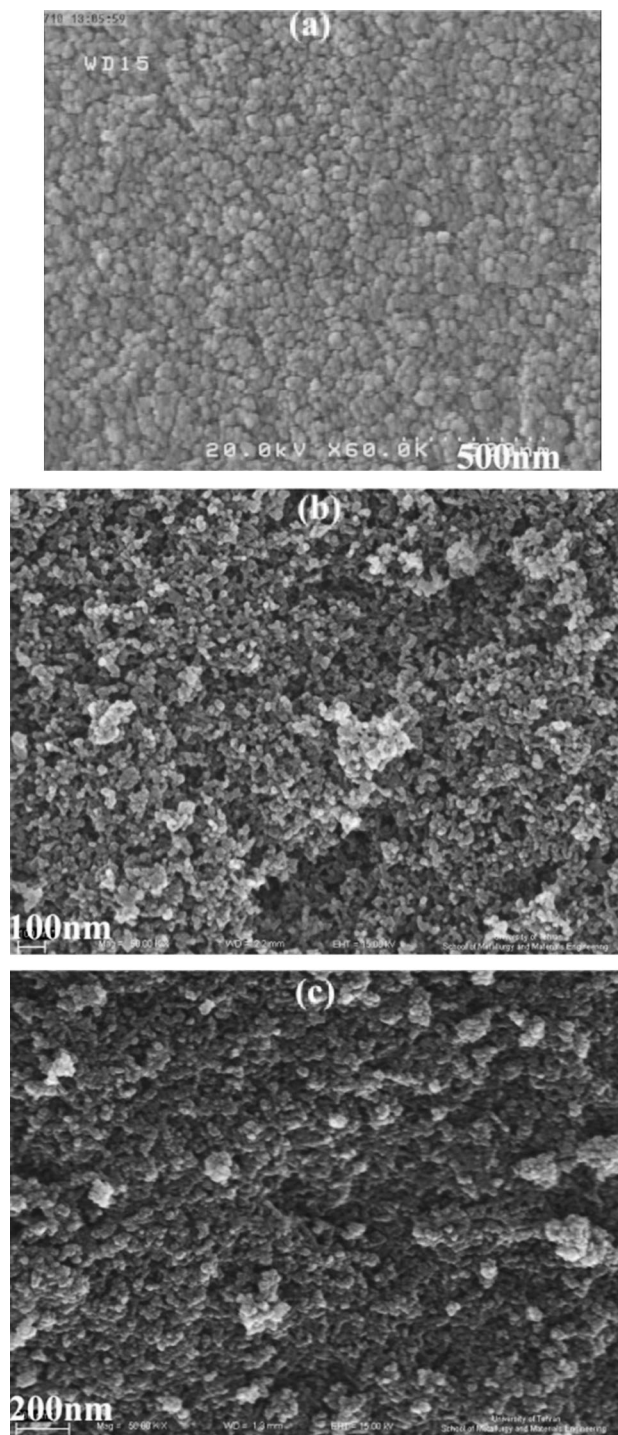
$$\alpha = \frac{\alpha_0 \left(h\vartheta - E_g \right)^n}{h\vartheta} \tag{1}$$

Fig. 3 SEM images of prepared **a** SiO_2, **b** TiO_2 and **c** $SiO_2@TiO_2$

where α is absorption coefficient, $h\vartheta$ is the photon energy, α_0 and h are the constants, E_g is the optical band gap of the material, and n depends on the type of electronic transition and can be any value between ½ and 3 [56]. The energy gaps of the samples have been determined by extrapolating

the linear portion of the plots of $(\alpha h\vartheta)^{1/2}$ against ht to the energy axis (Fig. 5) [57–59]. The E_g values have been calculated 3.8, 3.1, and 5 eV for the SiO_2, TiO_2, and $TiO_2@SiO_2$ core/shell nanoparticles, respectively.

3.5 TEM images

Figure 6 shows the representative HRTEM of $TiO_2@SiO_2$ core/shell nanoparticles. The obvious shell-core structure has been shown for $TiO_2@SiO_2$, indicating that the homogeneous coverage happened between SiO_2 and TiO_2 (Fig. 6). In the HRTEM, the ordered crystal lattices and amorphous structure have been shown in the core and shell of $TiO_2@SiO_2$, respectively. This indicated the core and shell of $TiO_2@SiO_2$ was TiO_2 and SiO_2, respectively. The SiO_2-coated TiO_2 was obtained. It has been shown in the HRTEM the average thickness of the SiO_2 coating layer was 3–8 nm.
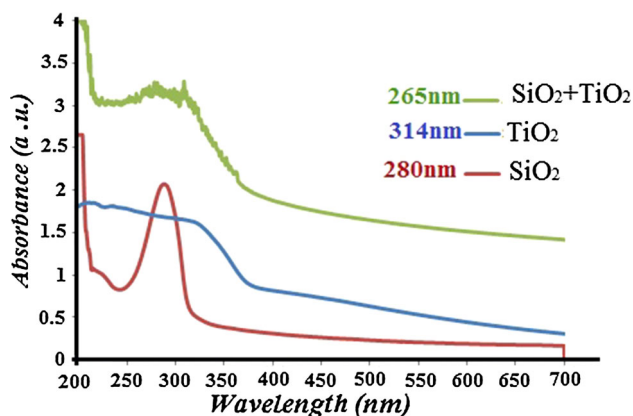

Fig. 4 UV–Vis diffuse absorption spectra of prepared (*red line*) SiO_2, (*blue line*) TiO_2 and (*green line*) $SiO_2@TiO_2$ (Color figure online)

3.6 Photocatalytic decolorization of MB dye

The photocatalytic activity of the nanoparticles was evaluated by monitoring the degradation of methyl blue (MB) in an aqueous solution, under irradiation with UV light (Fig. 7). Without light or nanoparticles, nearly no MB was broken down after 16 min, revealing that the contribution of self-degradation was insignificant. However, $TiO_2@SiO_2$ core/shell nanoparticles showed much higher

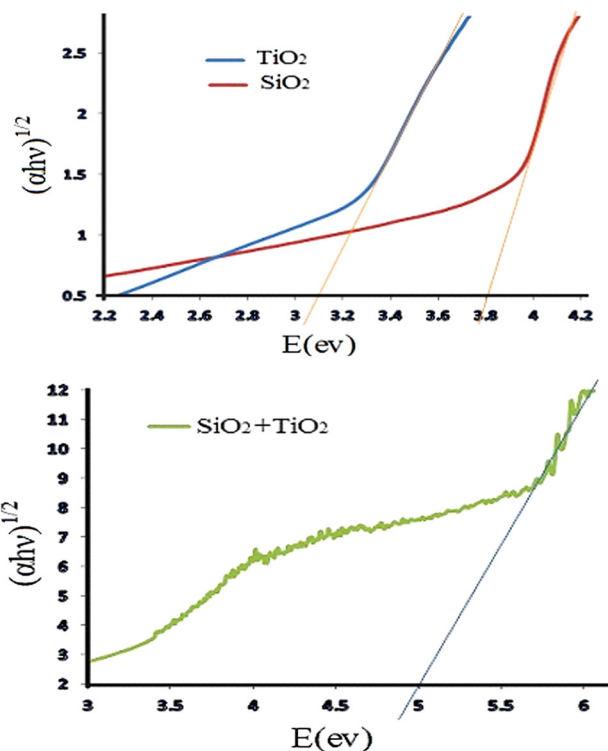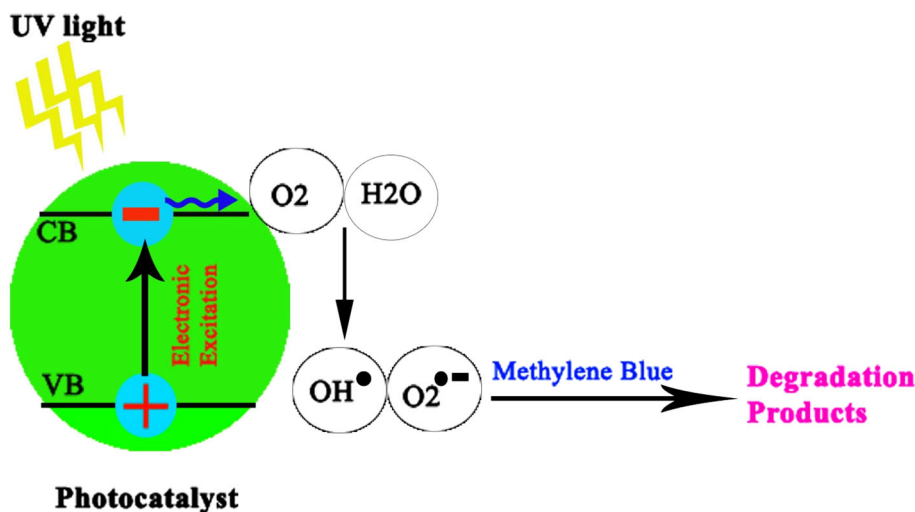**Fig. 5** The corresponding linear portion of the plots of $(\alpha h\vartheta)^{1/2}$ against $h\vartheta$

Scheme 1 Reaction mechanism of photocatalytic degradation of MB dye over $TiO_2@SiO_2$ core/shell nanoparticles under UV light irradiation

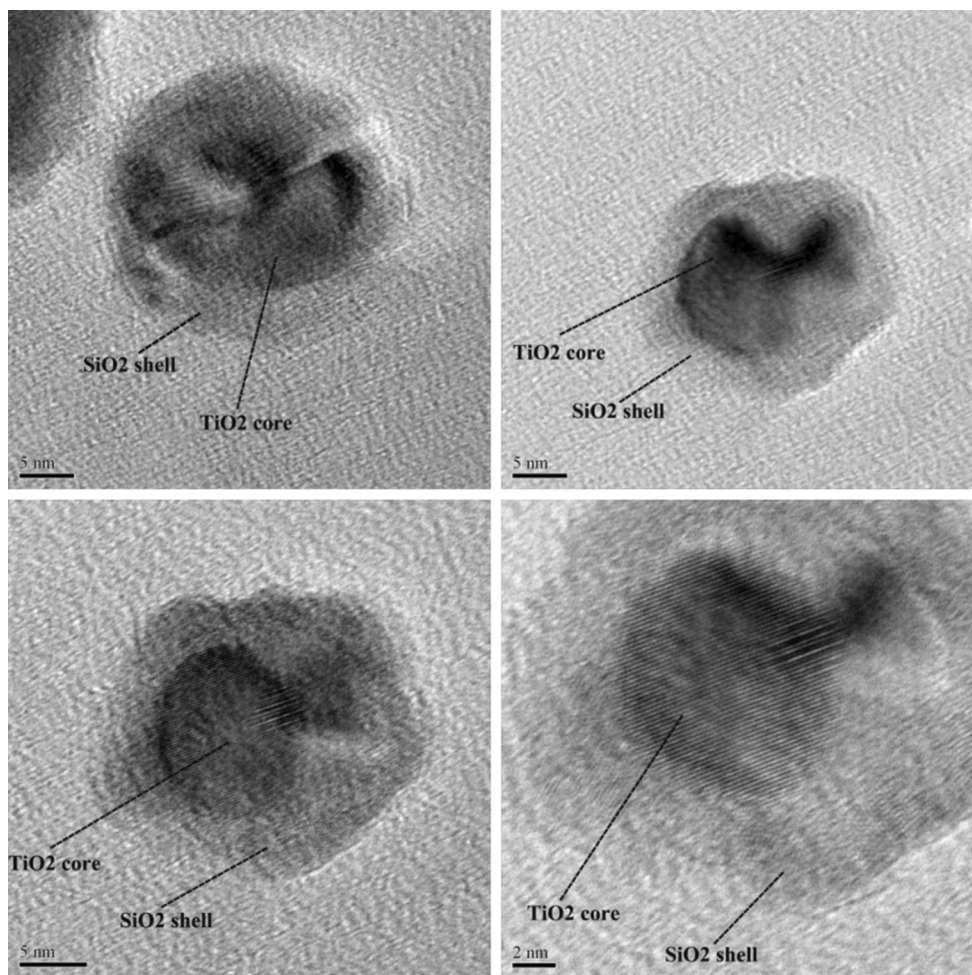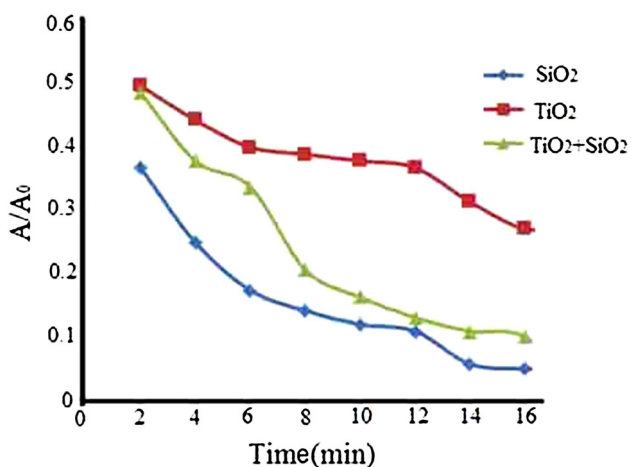**Fig. 6** HRTEM of TiO$_2$@SiO$_2$ core/shell nanoparticles

Fig. 7 Decolorization of MB dye of SiO$_2$, TiO$_2$ and TiO$_2$@SiO$_2$ core/shell nanoparticles

photocatalytic activity than TiO$_2$ and SiO$_2$ nanoparticles. The percentage of degradation $D\%$ was determined as follows:

$$D\% = \frac{A_0 - A}{A_0} \times 100 \qquad (2)$$

where A_0 and A are the absorbencies of the liquid sample before and after degradation, respectively. About 95, 89 and 68 % MB were degraded after 16 min for TiO$_2$@SiO$_2$ core/shell, TiO$_2$ and SiO$_2$ nanoparticles, respectively.

In spite of higher MB adsorption of TiO$_2$ nanoparticles than TiO$_2$@SiO$_2$ core/shell nanoparticles (Fig. 7), TiO$_2$@SiO$_2$ core/shell nanoparticles showed much higher photocatalytic activity. This probably causes the low recombination rate of photogenerated electrons and holes in TiO$_2$@SiO$_2$ core/shell nanoparticles [60]. The photocatalysis degradation is suggested to include the production of an (e$^-$/h$^+$) pair, leading to the formation of hydroxyl radicals ($^\cdot$OH) and superoxide radical anions (O$_2^{\cdot-}$). These radicals are the oxidizing species in the photocatalytic oxidation procedures. High separation rate of photo induced charge carriers are favorable to shape these radicals. We give some proposal to improve the photocatalytic efficiency in the future in such as: utilizing other metal oxide

semiconductors, adding other semiconductors to TiO_2@-SiO_2 core/shell nanoparticles and preparation TiO_2@SiO_2 core/shell nanoparticles by various chemical methods.

4 Conclusion

TiO_2@SiO_2 core/shell nanoparticles with enhanced photocatalytic activity under UV light were prepared by sol–gel method. TiO_2@SiO_2 core/shell nanoparticles exhibited much higher photocatalytic activity than SiO_2 and TiO_2 under UV light. Such outstanding photocatalytic activity of TiO_2@SiO_2 core/shell nanoparticles can be attributed to the increased adsorption of organic substrate and the low recombination rate of photogenerated electrons and holes.

References

1. M. Stylidi, D.I. Kondarides, X.E. Verykios, Appl. Catal. B **40**, 271 (2003)
2. J.B. Zhong, J.Z. Li, F.M. Feng, Y. Lu, J. Zeng, W. Hu, Z. Tang, J. Mol. Catal. A Chem. **357**, 101 (2012)
3. H.O. Seo, C.W. Sim, K.-D. Kim, Y.D. Kim, D.C. Lim, Chem. Eng. J. **183**, 381 (2012)
4. T.S. Sreeprasad, S.M. Maliyekkal, K.P. Lisha, T. Pradeep, J. Hazard. Mater. **186**, 921 (2011)
5. D. Zhao, M. Jaroniec, B.S. Hsiao, Editorial for themed issue on advanced materials in water treatments. Mater. Chem. **20**, 4476 (2010)
6. H. Ma, C. Burger, B.S. Hsiao, B. Chu, J. Mater. Chem. **21**, 7507 (2011)
7. J.H. Pan, H. Dou, Z. Xiong, C. Xu, J. Ma, X.S. Zhao, J. Mater. Chem. **20**, 4512 (2010)
8. N.K. Dey, M.J. Kim, K.D. Kim, H.O. Seo, D. Kim, Y.D. Kim, D.C. Lim, K.H. Lee, J. Mol. Catal. A Chem. **337**, 33 (2011)
9. Z. Ding, X.J. Hu, G.Q. Lu, P.L. Yue, P.F. Greenfield, Langmuir **16**, 6216 (2000)
10. S. Dutta, S.A. Parsons, C. Bhattacharjee, P. Jarvis, S. Datta, S. Bandyopadhyay, Chem. Eng. J. **155**, 674 (2009)
11. T. Robinson, B. Chandran, P. Nigam, Environ. Int. **28**, 29 (2002)
12. A. Ozer, G.B. Dursun, J. Hazard. Mater. **146**, 262 (2007)
13. D. Ozer, G.B. Dursun, A. Ozer, J. Hazard. Mater. **144**, 171 (2007)
14. F. Han, V.S.R. Kambala, M. Srinivasan, D. Rajarathnam, R. Naidu, Appl. Catal. A **359**, 25 (2009)
15. Z.G. Xiong, J.Z. Ma, W.J. Ng, T.D. Waite, X.S. Zhao, Water Res. **45**, 2095 (2011)
16. D. Yang, T. Fan, H. Zhou, J. Ding, D. Zhang, PLoS ONE **6**, e24788 (2011)
17. T.-X. Fan, S.-K. Chow, D. Zhang, Prog. Mater Sci. **54**, 542 (2009)
18. S. Gardin, R. Signorini, A. Pistore, G.D. Giustina, G. Brusatin, M. Guglielmi, R. Bozio, J. Phys. Chem. C **114**, 7646 (2010)
19. J.H. Mo, Y.P. Zhang, Q.J. Xu, J.J. Lamson, R.Y. Zhao, Atmos. Environ. **43**, 2229 (2009)
20. C. Euvananont, C. Junin, K. Inpor, P. Limthongkul, C. Thanachayanont, Ceram. Interfaces **34**, 1067 (2008)
21. G.D. Sheng, J.X. Li, S.W. Wang, X.K. Wang, Prog. Chem. **21**, 2492 (2009)
22. T. Guo, Z. Bai, C. Wu, T. Zhu, Appl. Catal. B **79**, 171 (2008)
23. J.M. Coronado, J. Soria, Catal. Today **123**, 37 (2007)
24. L. Cao, Z. Gao, S.L. Suib, T.N. Obee, S.O. Hay, J.D. Freihaut, J. Catal. **196**, 253 (2000)
25. M.R. Hoffmann, S.T. Martin, W. Choi, D.W. Bahnemann, Chem. Rev. **95**, 69 (1995)
26. J.T. Yates Jr, Surf. Sci. **603**, 1605 (2009)
27. C.-S. Kim, J.-W. Shin, S.-H. An, H.-D. Jang, T.-O. Kim, Chem. Eng. J. **204–206**, 40 (2012)
28. S. Cao, K.L. Yeung, J.K.C. Kwan, P.M.T. To, S.C.T. Yu, Appl. Catal. B Environ. **86**, 127 (2009)
29. R.N. Viswanath, S. Ramasamy, Colloids Surf. A **133**, 49 (1998)
30. X. Fu, L.A. Lark, Q. Yang, M.A. Anderson, Environ. Sci. Technol. **30**, 647 (1996)
31. P. Cheng, M. Zheng, Y. Jin, Q. Huang, M. Gu, Mater. Lett. **57**, 2989 (2003)
32. C. Jin, R.Y. Zheng, Y. Guo, J.L. Xie, Y.X. Zhu, Y.C. Xie, J. Mol. Catal. A Chem. **313**, 44 (2009)
33. C. Chen, M. Long, H. Zeng, W. Cai, B. Zhou, J. Zhang, Y. Wu, D. Ding, D. Wu, J. Mol. Catal. A Chem. **314**, 35 (2009)
34. G. Colón, M.C. Hidalgo, J.A. Navío, Catal. Today **76**, 91 (2002)
35. Z. Zang, X. Tang, J. Alloys. Compd. **619**, 98 (2015)
36. L. Hongjun, Z. Zang, X. Tang, Opt. Mater. Express **4**, 1762 (2014)
37. S. Lee, I.-S. Cho, J.H. Lee, D.H. Kim, D.W. Kim, J.Y. Kim, H. Shin, J.-K. Lee, H.S. Jung, N.-G. Park, K. Kim, M.J. Ko, K.S. Hong, Chem. Mater. **22**, 1958 (2010)
38. T. Sugimoto, X. Zhou, A. Muramatsu, J. Colloid Interface Sci. **259**, 53 (2003)
39. M. Gholami, M. Salavati-Niasari, M. Bazarganipour, E. Noori, Superlattices Microstruct. **61**, 33 (2013)
40. E. Noori, M. Bazarganipour, M. Salavati-Niasari, T. Gholami, J. Clust. Sci. **24**, 1171 (2013)
41. Z. Shahri, M. Bazarganipour, M. Salavati-Niasari, Superlattices Microstruct. **63**, 258 (2013)
42. M. Salavati-Niasari, B. Shoshtari-Yeganeh, M. Bazarganipour, Superlattices Microstruct. **58**, 20 (2013)
43. M. Bazarganipour, M. Salavati-Niasari, Micro Nano Lett. **7**, 388 (2012)
44. M. Salavati-Niasari, M. Bazarganipour, J. Clust. Sci. **23**, 503 (2012)
45. M. Goudarzi, M. Bazarganipour, M. Salavati-Niasari, RSC Adv. **4**, 46517 (2014)
46. S. Mandizadeh, M. Bazarganipour, M. Salavati-Niasari, Ceram. Int. **40**, 15685 (2014)
47. M. Ghaed-Amini, M. Bazarganipour, M. Salavati-Niasari, J. Ind. Eng. Chem. **21**, 1089 (2015)
48. S. Gholamrezaei, M. Salavati-Niasari, M. Bazarganipour, M. Panahi-Kalamuei, S. Bagheri, Adv. Powder Technol. **25**, 1585 (2014)
49. P.D. Cozzoli, A. Kornowski, H. Weller, J. Am. Chem. Soc. **125**, 14539 (2003)
50. S. Pradhan, S. Chen, J. Zou, S.M. Kauzlarich, J. Phys. Chem. C **112**, 13292 (2008)
51. G.-L. Tan, M.F. Lemon, R.H. French, J. Am. Ceram. Soc. **86**, 1885 (2003)
52. P. Klankaw, C. Chawengkijwanich, N. Grisdanurak, S. Chiarakorn, Superlattices Microstruct. **51**, 343 (2012)
53. X. Gao, I.E. Wachs, Catal. Today **51**, 233 (1999)
54. R.V. Grieken, J. Aguado, M.J. López-Muñoz, J. Marugán, J. Photochem. Photobiol. A **148**, 315 (2002)
55. Y.H. Hsien, C.F. Chang, Y.H. Chen, S. Cheng, Appl. Catal. B **31**, 241 (2001)

56. J. Tauc, R. Grigorovici, A. Vancu, J. Phys. Status Solidi B **15**, 627 (1966)

57. M. Abaker, A. Umar, S. Baskoutas, G.N. Dar, S.A. Zaidi, S.A. Al-Sayari, A. Al-Hajry, S.H. Kim, S.W. Hwang, J. Phys. D Appl. Phys. **44**, 425401 (2011)

58. M. Abaker, A. Umar, S. Baskoutas, S.H. Kim, S.W. Hwang, J. Phys. D Appl. Phys. **44**, 155405 (2011)

59. A. Umar, M. Abaker, M. Faisal, S.W. Hwang, S. Baskoutas, S.A. Al-Sayari, J. Nanosci. Nanotechnol. **11**, 3474 (2011)

60. S. Hu, F. Li, Z. Fan, Bull. Korean Chem. Soc. **33**, 1895 (2012)